

Dynamic Network-Code Design for Satellite Networks

I. Shrem, B. Grinboim, and O. Amrani

Abstract

Internet access from space enjoys renaissance as satellites in Mega-Constellations is no longer fictitious. Network capacity, subject to power and computational complexity constraints among other challenges, is a major goal in this type of networks. This work studies Network Coding in the presence of dynamically changing network conditions. The notion of *generalized acyclic network* is introduced and employed for promoting the generation of linear-multicast network code for what is considered to be a cyclic network. The performance of several network coding schemes, among these is the known *static network code*, is evaluated by a STK simulation for a swarm of communicating satellites, conceptually based on the Iridium system. Exploiting the prior knowledge of the networks topology over time, new network coding approaches are described, whose aim is to better cope with the time-varying, dynamic behavior of the network. It is demonstrated that in all cases, pertaining to our example network, static network codes under-perform compared to the presented approach. In addition, an efficient test for identifying the most appropriate coding approach is presented.

I. INTRODUCTION

Satellite communication networks, and in particular integrated information networks between space and earth, are increasingly deployed to serve in various aspects of life. Until recently, most of the communications among these satellites have been predominantly based on relaying via terrestrial base stations. Ignoring the potential resource, namely the inter satellite links (ISL), results in an atrophied network. Such satellite networks can not meet today's growing wireless communication needs. One of the canonical examples of this kind, relates to the idea of providing Internet services from space using Low-Earth Orbit (LEO) satellites, an idea that had regained popularity in recent years [13]. This renaissance may be attributed to developments in technology and sophisticated digital communication schemes, combined with the reduced costs of satellite development and launching costs known to fuel the "New-Space" revolution. As always, power consumption and communication throughput is a main concern [15],[11].

Figure 1: Butterfly network without network coding

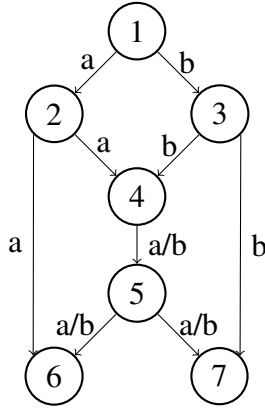
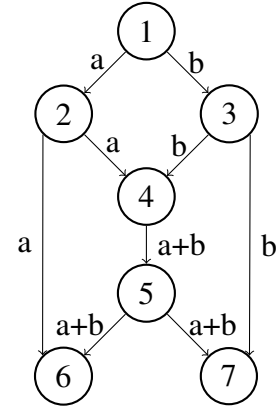


Figure 2: Butterfly network with network coding



Network coding is a research field targeting the improvement of communications within a network. The fundamental idea, discussed in [1], is that intermediate nodes in the network serve as computational units rather than merely relays, thus promoting increased overall network throughput. Network coding has been shown to potentially increase overall network throughput in single-source multiple-sink communications scenarios (i.e., broadcast of messages), or multi-source networks[9], [18], [6]. One of the fundamental results in this field is that in the case of a single-source, acyclic, and finite network, given that all computations are done over a field large enough, a *linear network code* (LNC) can achieve the maximum capacity to every *eligible sink* [9], [8]. By eligible sink, we mean a sink whose max-flow (achievable throughput) is greater or equal to the source transmission-rate.

A simple example demonstrating the strength of network coding is the so-called butterfly network, as demonstrated in Figures 1 and 2. Therein, two signals, a and b , are transmitted towards two sinks, 6 and 7. In Figure 1, the network does not employ network coding (i.e., intermediate nodes do not execute any coding-related computations) - hence only one of the sinks, either 6 or 7, can decode both messages in each network use. In Figure 2, the network employs network coding. To this end, node 4 performs bit-wise XOR (exclusive-or) on both its inputs, which in turn enables both sinks to decode the two transmitted messages.

Through the years, significant research efforts have been devoted to the subject of linear

network codes for acyclic and finite networks with a single communication source. Common classification of such networks is to linear multicast, broadcast, dispersion and generic.

Additional researched classes of LNC include *static LNC* and *variable-rate LNC*. With respect to static network codes, given a set of diverse network configurations (typically relating to commonly expected link failures), the eligible sinks in any of these configurations can still recover the source messages [8], [4], without having to change the network code whenever the network configuration changes. In variable-rate network codes, the source can generate messages at various different rates, again, without having to modify the network code itself [4].

Facilitating network coding in nano-satellite-based networks is particularly desirable as it allows the overall network capacity to improve without having to increase the power consumption - a scarce resource when it comes to nano-satellites. This may be possible, since the end-to-end topology of the network is known to the network planner and hence accessible to the operator. Moreover, since the satellite-network dynamics is typically known (based on Kepler's laws), **future** topology of the network is also predictable. Note that we assume that the topology and dynamics are only known to the operator. On the other hand, the satellite network dynamics poses a challenge to the classical network-coding approach, which has to be carefully tailored.

To address this challenge and provide practical tools and recommendations to network planners, we introduce a network coding implementation for a sample satellite network. Our network is conceptually based on the Iridium system - one of the most prominent test-cases of a satellite communication network [16], [14]. While Iridium is not planned as a network of small satellites, the results and methods presented herein are readily applicable to any satellite network (our sample network is based on Iridium in most of the satellites parameters).

The rest of the paper is organized as follows. Section 2 describes the network modeling and simulation environment. The following sections provide a step-by-step implementation of the proposed LNC for an Iridium-based network. Section 3 describes the first step of the LNC construction: path finding. Section 4 details the basic LNC algorithm construction. In section 5, a few different approaches for dealing with the network's dynamics are considered and compared. Section 6 concludes the paper.

II. MODELING THE NETWORK

Global satellite networks have been around since the 1990's to provide world-wide communications; among these are the Iridium and GlobStar-Immersat. Notably, the satellite itself, being one of the main factors in the overall cost of a satellite network, has a major impact on the service charges.

In recent years, nano-satellite networks are planned with the aim of significantly reducing overall costs, allowing this type of enterprises to be lucrative. Nano-satellites, a.k.a. "CubeSats", are very small ($1U = 10cm \times 10cm \times 10cm$), and weigh around $1kg$, considerably reducing launching costs, and allowing dozens of satellites to be launched into space together, on a single launcher. In addition, since nominal orbital altitudes of nano-satellites are much lower than existing satellite networks, its components, including some of the communication ingredients, does not necessitate "space grade" qualification.

In this section we shall introduce the common methodologies used to simulate and research cubeSat networks. In addition, we shall present the model built specifically for testing and challenging the concept of implementing a network code over a satellite based network.

A. Satellite Constellations & Simulations

A trade-off to consider when planning a satellite network is coverage vs. costs. As the launching constitutes a main cost factor, reducing the number of launches, and hence also the number of constellation orbital planes, is a common tactic. The main downside of such tactic is the relatively sparse coverage it provides. A possible solution is to create a cluster of satellites that only requires a small number of planes with a specific zone covered. This method is also considered for deep-space missions.

Superior coverage can be obtained by grouping satellites in different planes. In the industry, the first planned constellation was Iridium which initially targeted 7 planes and 77 satellites; eventually, 6 planes with 66 satellites was sufficient for providing the needed coverage. The main shortcoming of employing CubeSats for providing coverage is the orbital radius. Since the power available in a CubeSat is considerably smaller than in Iridium satellite, link-budget considerations

necessitate launching CubeSats to lower orbital radius. This, in-turn, means smaller coverage per CubeSat, so that additional orbital planes are necessary to achieve a desired coverage.

B. Link Analysis

In general, there are 3 principle link types in a CubeSat network (or any other satellite network for that matter) : *uplink* for transmitting commands from the ground station (GS) to the satellite, *downlink* for transmitting data to the GS, and *ISL* for transmitting data among satellites. The *propagation path loss*, depends mainly on the distance r between the communicating nodes, and the frequency used for the transmission.

1) *Link Budget*: To lay down the conventions and assumptions for link budget calculations of a cubeSats network, we reviewed existing and future-planned cubeSat network enterprises (see e.g. [12], [15]). Our findings are summarized below.

- 1) **Distance** - The distance r between the different transceivers (CubeSat - GS, CubeSat - CubeSat) is determined by the orbital parameters of the CubeSat's constellation.
 - a) The distance between the ground station and a CubeSat is determined by the orbit trajectory pole and effective horizon; nominally in CubeSats constellations $100_{km} \leq r_{GS-Sat} \leq 2000_{km}$.
 - b) The distance between CubeSats varies quite considerably for different constellations (inter-plane and intra-plane links) : $10_{km} \leq r_{ISL} \leq 1000_{km}$.
- 2) **Frequency** - CubeSats typically use frequencies in the VHF and UHF bands for earth-satellites communications due to 2 main reasons:
 - a) Use of unlicensed amateur radio frequencies in the VHF bands (144 MHz to 148 MHz) and UHF bands (420 MHz to 450 MHz).
 - b) Relatively small atmospheric attenuation which benefits the link budget.

CubeSat planners usually use L or S band for ISL communications. This is due to the relatively small path loss, and because the corresponding wavelength is short enough so that building a directed patch antenna with a gain of $5 - 6dBi$ is feasible.

3) **SNR** - For digital modulation schemes, the SNR at the receiver is given by the ratio $SNR = E_b/N_0$, where E_b , the energy per bit, is given by $E_b = P_r/R$ with P_r being the received Power, and R the data rate in bits per second [bps]. The noise spectral density N_0 is expressed by $N_0 = k_b T_s$ where T_s is the system noise temperature, and k_b is Boltzmann's constant. Determining the system temperature is not a trivial task since CubeSats are not radiation protected, and the systems temperature can vary between $100 \leq T_s \leq 1000 [^\circ K]$. The model used for calculating path losses in such links is the *free space loss* (FSL) L_p . It is given by $L_p = (\frac{4\pi df}{c})^2$, where d denotes the distance between the transceivers, f the operating frequency and c the speed of light. The SNR is then given by:

$$SNR = E_b/N_0 = \frac{P_t G_t G_r}{k_b T_s R L_p} \quad (1)$$

where G_t, G_r denote the transmission and reception antenna gains, respectively. It is common to state the equation in the logarithmic domain: $SNR = P_t + G_t + G_r - L_p - 10 \log_{10} k_b - 10 \log_{10} T - 10 \log_{10} R$, where P_t, G_t, G_r, L_p are given in dB.

2) *Transceiver & Front End Section*: Communicating data between CubeSats requires a simple and power-efficient baseband signal processing scheme. [12], [15], [11] present the properties of the communication channel alongside the requirements, limitations, and today's common practice among nano satellites. A digital modulation method suitable for CubeSat missions is frequency shift keying (FSK) or binary phase shift keying (BPSK), which has been used with other low-power low-data rate applications. Notably, the bit error probability associated with such modulation techniques is relatively small even in low SNRs typical for these types of links. In addition, BPSK/BFSK are very simple to implement, hence facilitating the use of COTS (commercial off-the-shelf) components, such as low power consuming modulators/demodulators. The main shortcoming of this digital scheme is that the supported rate is low, hence severely limiting the amount of data that can be sent in the short time-period a CubeSat is visible from the ground station.

Often CubeSats do not have angular orientation control (due to limited available power/size/weight), which necessitates the use of a wide coverage, omni-directional or hemispherical

antenna. This naturally comes at the price of relatively low antenna gain. In addition, power amplification is scarce due to power/weight constraints, the commonly used transmit power, p_t , at the CubeSat side is $15_{[dBm]} \leq p_t \leq 30_{[dBm]}$.

For the ground station the conditions are much less restrictive, typical parameters for the antenna gain and transmission power are - $G_{GS} = 15dBi$ (for a Yagi antenna), and $40_{dBm} \leq p_t \leq 50_{dBm}$, respectively

Table I summarizes some typical parameters:

Table I: Power Budget Conclusion

	(a) Inter Satellite Links		(b) Up/Down Links		
	L - band	S-band		Uplink	Downlink
$f[GHz]$	1.2	2.4	$f[GHz]$	437	146
$p_t[dBm]$	15	15	$p_t[dBm]$	15	50
$G_t[dBi]$	5	5	$G_t[dBi]$	15	0
$G_r[dBi]$	5	5	$G_r[dBi]$	0	13
$L_p[dB]$	115	120	$L_p[dB]$	144	154
Noise Figure $N_f[dB]$	3	3	Noise Figure $N_f[dB]$	2	5
$T_s[^\circ K]$	1200	1200	$T_s[^\circ K]$	1000	1000
$R[bps]$	3M	1M	$R[bps]$	2400	1 M
$SNR[dB]$	10	9	$SNR[dB]$	12.7	11.35

C. Modeling the Test Network

This subsection considers the different assumptions and methods used to generate our “sandbox” network. In the absence of an available model for LEO cubeSat network, constructing a realistic model to test the utilization of a network code in a cubeSat network is the first step. Our model combines the topology and *dynamics* of the Iridium satellite network with the *communication scheme* employed for cubeSat networks. We capitalize on two major characteristics of the Iridium network. First, is the network “density”: the Iridium network offers many potential links (especially ISLs). When examining a network as a graph, one can see that network coding is beneficial when the graph’s max-flow is sizable (with respect to a single link). Second, is the network dynamic behavior. Testing a network code in a dynamic network requires paying special attention to the state of all links at all times. We expect that the time-domain features of

the network topology will be the most significant factor when adapting the network-code to the changing network, hence the importance of modeling the **real** dynamics of the Iridium network.

Note that an inherent mismatch exists between the communication scheme of a $1 - 10Kg$ cubeSat and $680Kg$ Iridium satellite (especially with respect to transmission power and antenna sizes). In the following subsections we describe the Iridium dynamics and the communication-related adaptations made to tackle all these issues.

1) *Model Dynamics*: The Iridium network [14] is one of the most researched satellite communication networks among GNSS, and Globstar, making it a perfect basis for a test case, especially since there are no full-scale, fully developed nano-satellite networks today. The Iridium network is a LEO (low earth orbit) constellation, hence relevant to futuristic nano-satellite constellations (unlike GNSS which is MEO). the constellation consists of 66 satellites with $R_{earth}^{Iridium} \sim 780_{km}$, the satellites are evenly spaced in 6 different orbital planes spaced 30 degree apart, in 86 degree inclination. In addition, we assume 8 ground stations in different locations around the globe so as to examine the earth segment influence on the entire network (symmetry, Doppler, line of sight, etc.). Lastly, the constellation's dynamic was modeled during 24 hours using the mentioned constellation parameters with simulation timestamp $\Delta t_{timeStep} = 1_{min}$. It is important to note that the satellite's angular dynamics was neglected .

The complete network behavior has been projected onto a 3D matrix, $Range$, detailing all the possible links over time, as they are affected by the constellation's dynamics and the existence of a line-of-sight (LOS) between a pair of satellites. The value of the cell $Range_{i,j}(t)$ denotes the distance between node i and node j , t minutes from the beginning of a test scenario (When a communication link does not exist, the value is null):

$$Range(:, :, t) = \begin{pmatrix} Range_{1,1}(t) & \cdots & Range_{1,66}(t) \\ \vdots & \ddots & \vdots \\ Range_{66,1}(t) & \cdots & Range_{66,66}(t) \end{pmatrix}$$

2) *Model Transceiver Section:* We emphasize that many communication-related aspects, such as coding, framing, congestion avoidance etc., are in fact transparent for the task at hand; as network code planners – the network code acts as an add-on that actually affects the communicated data itself and is independent of the connection methodology. The link parameters that will be considered are those relevant for the calculation of the link budget, and consequently determine the link existence.

Digital modulation: As stated above, simplicity and power efficiency are dominant factors when choosing a digital modulation scheme for CubeSats. In order to perform in the low SNR regime, and by that facilitate a dense network of nodes, we have chosen BPSK modulation.

Front End: Transmission power is crucial in any communications scheme, we choose $P_t = 30dBm$, which is the most powerful amplifier the literature mentions for cubeSats. Frequency selection for Inter-satellite links is also quite crucial for our model. L-band and S-band are the commonly mentioned as ISL frequencies in the literature. However, these frequencies are chosen with respect to $d_{sat-sat} \leq 2000Km$, which is not the case with Iridium where $1000km \leq d_{sat-sat} \leq 6000km$. [12] mentions that the link margin in the case of L-band ISL with data rate of $R = 10Kbps$, and $d_{sat-sat} \sim 100Km$ is less than $10db$ (hence, not adequate for reliable communication). Thus, using the same communications scheme in our model, with $d_{sat-sat} \sim 4000Km$ is impossible (assuming data rate $R = 10Kbps$). The cubeSat size and weight prevents us from increasing the transmission power, or changing the antenna - thus, there is no other choice but to use VHF frequency for the ISL as well with the same omni-directional antenna. It is important that since the Downlink and Uplink do not contribute much to the network's density, they were not fully modeled. Specifically, ground stations front end's are not different than satellites front end's (in terms of power amplifiers and antenna) in our model.

3) *Link Budget:* Iridium constellation consists of 3 link types: Uplink, Downlink, ISL. Nevertheless, not all ISL are legitimate in Iridium (even if they meet LOS and SNR requirements). As explained, one of the main objectives of this model, is creating as dens of a network as possible, thus embracing VHF links as previously justified. The main influence of this implementation (i.e using only VHF communications), is that the dominant factor influencing the link budget is

Table II: Satellite communication modeled parameters (all link types)

parameter	value
$f_c [MHz]$	146
$R [Kbps]$ (per FDMA channel)	6.4
$T [^\circ K]$	1000
$G_r [dBi]$	0
$G_t [dBi]$	0
$P_t [dBm]$	30

solely the range between two nodes, disabling the traditional preference of Uplinks/Downlinks in satellite communication (mainly thanks to high-gain ground station antennas) causing a higher network symmetry.

Now, after presenting all assumptions for the communication scheme, we can define and stock a so-called *link budget matrix* and derive the link capacities according to Shannon–Hartley’s Theorem and Equation 1.

The resultant network matrix holds the link capacities

$$C_{i,j} = BW \cdot \log(1 + SNR_{i,j}) \quad (2)$$

for any link between nodes i and j . We note that since the satellites antennae are omni directional, and the transmission powers are all the same, this matrix is symmetric. From this matrix, the transformation to a graph is simple - each satellite is a node, and the weights¹ of the connecting edges are given by $C_{i,j}$. Null $C_{i,j}$ means that there is no edge connecting node i to node j .

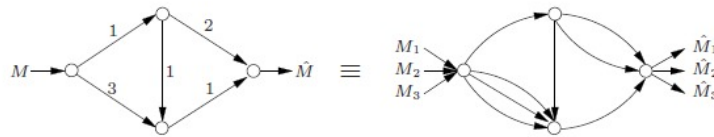
Finally, to be able to apply algorithms that require all edges of a graph to be unit capacity links, we needed to manipulate our weighted graph. To this end, the weighted graph is converted into a *multi-graph* by: 1. rounding down the capacity value of each edge, and 2. duplicating the unit capacity edge by the resulted integer capacity, as illustrated in Figure 3 [6].

III. INSTANTANEOUS NETWORK CODE IMPLEMENTATION

The algorithm for establishing a *linear network code* (LNC) consists of several steps:

¹we note here that greater weights indicate better communication link.

Figure 3: Integer Capacity Channels Modeling



- 1) An *acyclic* graph representation of the network G is given along with defined source node and set of designated sink nodes as introduced in the previous section;
- 2) The network's (G 's) max-flow, h , from the source to the designated sinks is derived, and h independent paths between the source and each designated sink are identified;
- 3) The paths found in Step 2 are used: the network nodes are examined in an upstream-to-downstream order, and for each node all its outgoing edges are examined separately in an arbitrary order: The *Global Encoding Kernel* (GEK) for each edge is calculated so that it satisfies the conditions in 1. This guarantees that the input to each of the designated sinks is decodable.

Steps 2 and 3 will be thoroughly explained in the Subsections 3.1 and 3.2. Subsection 3.3 introduces the concept of *cyclic network codes* (CNC) for *cyclic* graphs.

A network node in G that is neither source, nor sink, shall be called an “intermediate node”.

A “path” is a set of links that provides a connection between two nodes in the network.

A. LNC on acyclic graphs.

Consider a network $G' = \{V, E\}$, with V and E denoting network nodes and links (alternative terms for vertices and edges as we are dealing with a communication network), respectively; a source node s in V and a set of d sink nodes $T = \{t_1, \dots, t_d\}$ in V . The max-flow between s and $t_i \in T$ is denoted by h_{t_i} ; in this paper, the term “max-flow” of a sink t_i shall always refer to this h_{t_i} . All the information symbols are regarded as elements of a base field F (this terminology is often referred to as *scalar network codes*).

The operation *rate* of the communication network, denoted by r , is a positive integer representing the number of symbols created by the source every network use. In this paper, assume that r is constant.

For every node $x \in V \setminus \{s\}$, denote by $In(x)$ and $Out(x)$ the sets of input and output edges to the node x , respectively. For convenience, it is customary to add another node s' , referred to as the *imaginary source*, that has r outgoing edges to the original source s - referred to as the r *imaginary links* (namely, $In(s)$ represents the set of r imaginary links). Assume that G' includes the imaginary source associated edges.

The basic concept of network coding is that all the nodes in the network are able to perform calculations over the field F .

The following is a description of a *linear network code* that is derived from [18]:

Definition 1. An r -dimensional F -valued linear network code operating in an acyclic communication network is characterized by:

- 1) *Local Encoding Kernel (LEK)* - $\{k_{d,e}\}$ - A set of scalars $k_{d,e} \in F$, one for every adjacent pair of edges (d, e) in the network, where $d \in In(x)$ and $e \in Out(x)$;
- 2) *Global Encoding Kernel (GEK)* - $\{f_e\}_{e \in E}$ - A set of r -dimensional column vectors f_e , one for every edge e in the network such that:
 - a) For every non-source node x , and every $e \in Out(x)$, $f_e = \sum_{d \in In(x)} k_{d,e} f_d$;
 - b) For the imaginary links $e \in In(s)$, the set of vectors $\{f_e\}_{e \in In(s)}$ are defined as the r linearly independent vectors that constitute the natural basis of the vector space F^r .

The local encoding kernel associated with node x refers to a $|In(x)| \times |Out(x)|$ matrix. The vector f_e is called the global encoding kernel for edge e .

Note that given the local encoding kernels at all the nodes in an acyclic network, the global encoding kernels can be calculated recursively in an *upstream-to-downstream* order based on the given definition.

Definition 2. Let $\{f_e\}$ denote the global encoding kernels in an r -dimensional, F -valued, linear

network code in a single-source finite acyclic network. Let $V_x = \text{span}\{f_d | d \in \text{In}(x)\}$. Then, a linear network code is a *linear multicast* if $\dim(V_x) = r$ for every non-source node x satisfying $\text{max} - \text{flow}(x) \geq r$.

A known algorithm for constructing a linear multicast for a single-source finite acyclic network [9], [18] requires the field size $|F|$ to be greater than the size of the set of sinks (whose $\text{max} - \text{flow}(\{T\}) \geq r$) i.e, $|F| > |\{T : \text{maxflow}(\{T\}) \geq r\}|$. This algorithm provides a the LEK and GEK of a linear multicast on the graph, i.e. a LNC that allows all target sinks to receive decodable information simultaneously in every network use.

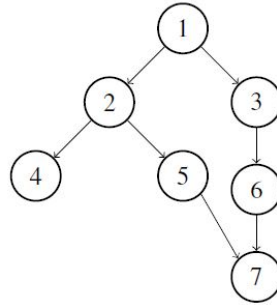
Definition 3. Let $G = (V, E)$ be a connected directed acyclic graph, and let $s \in V$ be a node in G , called the *source node*. Note that G is a tree, with s as its root. Denote $n = |V|$ as the number of nodes in G . An *upstream to downstream order* defines ordering of the nodes in V , $O : V \rightarrow \{1 : n\}$ in G , such that for every $v, u \in V$, if u is a parent of v in the tree induced by G , $O(v) > O(u)$, and for every $u_1 \neq u_2$, $O(u_1) \neq O(u_2)$. In other words, looking on O as an order of choosing the nodes, a node is chosen only after all of its parent nodes have been chosen. The order could also be denoted $O = \{v_1, \dots, v_n\}$, meaning that $O(v_i) = i$.

Example 4. Examine the graph G presented in Figure 4, and the orders $O_1 = \{1, 2, 3, 4, 5, 6, 7\}$, $O_2 = \{1, 2, 4, 5, 3, 6, 7\}$, $O_3 = \{1, 2, 4, 3, 5, 6, 7\}$ and $O_4 = \{1, 3, 6, 7, 2, 4, 5\}$. O_1 , O_2 and O_3 are all upstream-to-downstream orders - in all of them, the parents of every node comes prior to them in these orders. In contrary, O_4 is NOT an upstream-to-downstream order, since $O_4(7) < O_4(5)$, even though 5 is a parent of 7 in G .

B. Path Finding

This subsection will describe the methodology used finding *max-flow* different paths from the source s to the sinks T over the graph G . Path finding is needed in order to provide an ordered list that will enable calculating in an upstream to downstream order over the nodes as defined in Figure 4.

Given a graph G , our construction algorithm of the network code consists of two preliminary

Figure 4: An Example Graph G' 

steps; the first, calculating the *max-flow* of the graph. We used MATLAB's built-in function (based on Boykov-Kolmogorov algorithm [2]) in this implementation. The second, finding *max-flow* disjoint paths from the source s to each defined sink $t \in T$. Path-finding does not necessarily result unique paths selection for a specific configuration of source and sinks. To dissolve this ambiguity, the parameter taken into consideration inhere is the comparability to routing techniques. Since most routing algorithms base on shortest-path finding (using Dijkstra's algorithm for example), we employ the following shortest-path-based algorithm stated for a single source s , and single sink $t \in T$.

Algorithm 1 shortest path based path finding

```

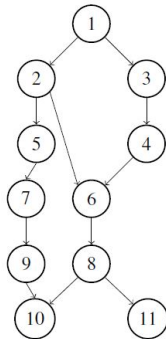
Initialization :
Paths = []; Network = G; Weights = {C(i,j)}; source = s, sink = t;
For i = 1: max-flow
    Paths(i) = Dijkstra(Network,s,t)
    // find shortest path to sink from source
    given the network Network

Weights(paths(i)) = Weights(paths(i)) -1 ;
// remove one edge from the multi-graph

If Weights(paths(i)) =0
    Network = Network \ Paths(i);
End
  
```

Assuming a Dijkstra based routing algorithm, one could simply compare the throughput at a

Figure 5: Shortest-Path based path-finding failure. The source node s is node #1, the algorithm fails to achieve 2 disjoint paths to sink #10.



sink t when using routing and network coding. However, as demonstrated in Example 5, our shortest-path-based search algorithm does not guarantee finding *max-flow* disjoint paths. We did not encounter a failure finding *max-flow* paths on the Iridium network for any topology tested (many variations over source and sinks selections). Nevertheless, a comparison of the number of paths found by the algorithm to the network's *max-flow* is a required sanity check.

If the check were to fail, we would have used the Ford-Fulkerson algorithm [5] (This algorithm guarantees finding disjoint *max-flow* paths). However, this algorithm does not necessarily find the shortest path, thus disabling the opportunity to compare our results to routing techniques.

After finding all *max-flow* paths, we will observe only the graph G' , which is a pruned version of the graph G after removing the edges that are not participating in any of the allocated paths. Such a graph G' will be referred to as a (pruned) paths-graph of the network G with respect to the source s and set of sinks T .

C. CNC on cyclic graphs.

In the case of a finite, single-source and *cyclic* network, it has been shown [10] that if the field F is large enough, there exists a Convolutional Network Code (CNC) achieving rate of r messages in each designated sink t . A designated sink is one with *max-flow* $h_t \geq r$; all the operations are done over the field F , and the vectors of the GEK are vectors in $F[D]^r$ (D being

a unit delay). In [3], a relatively efficient algorithm for finding such a CNC is presented – though it is of much higher complexity in comparison to the efficient LNC-finding algorithms. Consider that the higher complexity of such algorithms derives from the fact that in the absence of an upstream-to-downstream order on the nodes in cyclic networks, the algorithm has to visit every node several times to make sure that the linear independency is kept [3].

IV. LINEAR MULTICAST IN GENERALIZED ACYCLIC NETWORKS

A. Definition and Motivation

Continuing the previous section, with the aim of designing an efficient network code for the example network with a pruned paths-graph G' , it is necessary to determine whether G' is a cyclic or an acyclic graph. Seemingly, it is a simple problem; the original Iridium network, G , is obviously cyclic since all its channels are assumed to be full-duplex, meaning that every link is itself a cycle. Consequently, when considering the high connectivity and high max-flows of the example network as modeled, it is not difficult to realize that cycles in G' are created with almost any combination of sinks. Notwithstanding the above, since it is considerably more complex to construct a cyclic convolutional network code than a linear multicast code for an acyclic network, the motivation to somehow apply acyclic graph-methodologies is high. The problem is that finding an upstream-to-downstream order, which is an essential step of a linear multicast construction, is of course impossible on the cyclic graph G' . In some cases (which cases exactly - will be discussed later in that section), the network operation can be characterized as a degenerate version of a cyclic network, termed *generalized acyclicity*, which is sufficient for applying the methodologies of acyclic graphs. This characteristic and the relevant method to be applied is explained next.

Definition 5. Assume given a graph $G = (V, E)$ (for notational brevity, and w.l.o.g, assume that $G = G'$), a source node s , a set of sinks T and a choice of paths, denoted by P , from s to each sink in T . Let the *paths line-graph* (PLG) induced from G , with respect to the set of paths P , be the graph $LG = (LV, LE)$, with the *line-graph nodes* being $LV = \{s, T, E\}$, and *line-graph edges* $(e_1, e_2) = \epsilon \in LE$ if:

- 1) $e_1 = s, e_2 \in E$, where e_2 is an outgoing edge from s in G .
- 2) $e_2 = t \in T, e_1 \in E$, where e_1 is an incoming edge to t in G .
- 3) $e_1, e_2 \in E$ and a node $v \in V$ such that e_1, e_2 are an incoming edge to v and an outgoing edge from v respectively, and there exists a path in P that includes the transition from e_1 to e_2 via v .

This type of line-graph construction was introduced by Erez & Feder [3]. Note that a paths line-graph is not a conventional line-graph. PLG includes line-graph edges between the edges of the graph G only if the transition between the latter edges is included in a certain path, and only in the direction of a path. As a result, unlike conventional line-graph that preserves the cyclic (or acyclic) characteristics of the original graph – a paths line-graph may be acyclic also when the graph it is induced from is cyclic. This motivates the following definition:

Definition 6. Given a graph G , a source node s and a set of sinks T , G is a *generalized acyclic network* with respect to s and T , if there exists a set of max-flow paths P from s to each sink in T , so that the path line-graph induced from G , with respect to P , is acyclic.

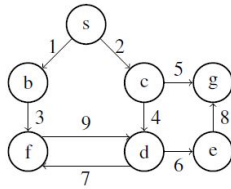
Note that every acyclic graph G is also generalized acyclic - since all its PLG are necessarily acyclic. The interesting case is hence the case in which a *cyclic* graph is generalized acyclic. Example 7 demonstrates such a case.

Example 7. Consider the graph G at the left-hand-side of Figure 6, with the node $s = 1$ as the source and nodes $T = \{6, 7\}$ as sinks. Not only G is a cyclic graph, it is also easy to see that both the edges $(4, 6)$ and $(6, 4)$ are necessary in order to achieve a communication rate of $max - flow = 2$ between s and T , and hence the paths-graph G' is also cyclic. The right-hand-side figure demonstrates a PLG of G . In this case, since there is only one choice of paths that achieves the max-flow to each of the sinks, this PLG is unique. Note that even though G' is cyclic, the PLG is acyclic, hence G is a generalized acyclic graph.

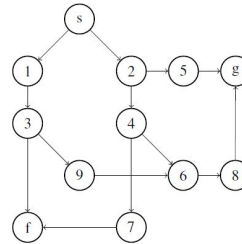
Theorem 8. *Given a generalized acyclic network G with source s and set of sinks T , there exists a linear multicast on G , if the messages and computations are carried out over a large*

Figure 6: Graphical demonstration for Example 7

(a) Original graph G . G is cyclic, but also generalized acyclic.



(b) PLG , the paths line-graph for G .



enough field.

The theorem is based on the ability to find an upstream-to-downstream order in the paths line-graph, which essentially allows to "break" cycles that exist in the original graph (but effectively not used by any combination of paths).

A constructive proof is next given in the form of an algorithm consisting of two stages:

- 1) Derivation of a modified version of linear multicast on the PLG ;
- 2) Conversion of modified version to a linear multicast on G .

Proof: Let LG be an acyclic PLG of G , with r being the operation rate of the network. Since LG is acyclic, it is possible to find an upstream-to-downstream order for its nodes going from s to T . Note that this does not necessarily induce an upstream-to-downstream order on the nodes of G . Next, the algorithm proceeds in a similar manner to the known linear multicast algorithm (see [9]).

For this process to yield a network code not only on the path graph but also on the original graph G , every LG -node (which is equivalent to an edge on the graph G) is only allowed to be associated with a single GEK, which is a F^r vector. This is different from the original algorithm in [9], according to which every edge is associated with a global encoding kernel - hence allowing every node to "hold" all the global encoding kernel values of incoming edges simultaneously. The LG -node GEK vector will be used for determining the GEK value of the equivalent graph G edge later in this algorithm.

For example, consider LG-node 6 in Figure 6, which has two incoming edges. If each node is allowed to hold more than one GEK vector, the conversion to a linear network code on G will not be straight forward. This is because 6 is an edge in the original graph G , and hence allowed to hold only a single GEK value according to definition 1.

This calls for a modification in the aforementioned algorithm ([9]): instead of running over the nodes and edges of the LG , the algorithm has to run only on its nodes. The paths for the modified algorithm are those induced by the paths of the original graph G .

Except for the source node s (which is treated separately), the modified algorithm guarantees that every node (anywhere) in the line-graph that leads to a non-empty subset of sinks $T' \subseteq T$ holds only one vector that satisfies two conditions:

- 1) It is linearly independent from the set of all the other vectors held by the nodes that are in paths to sinks in T' (for each $t' \in T'$ separately, of course). For every sink, there are exactly r such nodes, since they are induced by edges in r distinct paths to that sink.
- 2) It is a linear combination of the vectors held by its incoming edges.

The existence of such vectors is a straight-forward corollary from the original algorithm given for linear multicast [9].

Contrary to the original linear multicast algorithm ([9]), where each of the outgoing edges from a node may hold a different GEK, in the proposed algorithm all the edges coming out of a node share the same GEK; once the specific GEK vector of a node has been determined, all its outgoing edges obtain the same GEK value. Note that since the proposed algorithm operates in an upstream-to-downstream order, all the GEK values of incoming edges to a node are determined before calculating the node's GEK value.

As for the source node, the algorithm is initialized with the source incoming edges holding all the unit vectors of the r dimensional vector space. The values of its outgoing edges are not initialized, but rather determined based on the values of the other nodes connected to them (which are equivalent to the outgoing edges from the source in the original graph, so that they fulfill condition 1 above). Thus, each sink is receiving r linearly independent vectors, which means that a valid linear multicast on the LG is obtained in accordance with Definition 7.

Given the linear multicast on the LG with a single vector value for each and every node, conversion to a linear multicast on G is straight forward: the global encoding kernel of every edge $e \in E$, its will be the global encoding kernel of its equivalent LG-node. It follows directly from the construction of the linear multicast on the graph LG , that the result is indeed a linear multicast on G . ■

B. Algorithm Complexity Analysis

As expected - the computational complexity of the proposed algorithm is lower than the alternatives, as the latter involve the design of a cyclic network code. In [3], the complexity of finding a convolution network code for a cyclic network is $O(d^3|E|^{w+2})$ with $d = |T|$ and w is the exponent of multiplying two matrices which is known to be $2 \leq w < 2.37$. The efficiency of the algorithm presented here is identical to that of a regular linear multicast construction, which if implemented by the method shown in [7], is $O(|E|dh^2 + |E|hd^2)$ – the path-finding algorithm needs run only on the original graph, while the code construction is only carried out on the PLG. The LG construction is bounded by $|E| \cdot h$.

V. NETWORK CODE UNDER DYNAMIC NETWORK CONDITIONS

Up until this point the paper considered linear multicast for a snapshot, i.e. instantaneous setting, of the satellite constellation network. From now on, dynamic behavior of the network is considered to account for the constantly changing topology of the network. It is clear that applying the network code designed for a specific network topology on another topology may render the decoding in some sinks impossible. The network code must be properly adapted, and its parameters distributed among the relevant network nodes, whenever the network topology changes enough. Alternatively, one may try to come up with code constructions that are effective even under topology changes. In order to minimize the impact of network topology changes on communication performance, we shall utilize the fact that these changes may have predictable behavior. In this section, three coding methods that utilize this network behavior are described and compared.

- 1) **Instantaneous Network Code - Construction and distribution of a new network code with each network change.** Given that the topology of the entire network is only known to a ground station, this method calls for the distribution of tailored network code-parameters for each time interval - call it a 'Genie' approach. The distributed message size is $|V|^3 \cdot \log_2(|T| + 1)$; where $\log_2(|T| + 1)$ denotes the symbol rate, and $|V|^3$ amounts to choosing the triplet $(x, d = In(x), e = Out(x))$ (per node x). Assuming communication rate of $6.4Kbps$, and 66 satellites (as presented in chapter 2), the time for distributing the new parameters throughout the network is:

$$t_{distribution} = \frac{|V|^3 \cdot \log_2(|T| + 1)}{6400} [sec] \approx 44 \cdot |F| [sec] \quad (3)$$

. Given that the network topology changes every 60_{sec} , this approach is practically irrelevant. In this section, this method is, nevertheless, employed as upper bound. Note that if memory resources (at the network nodes) are abundant, and the network topology is truly periodic, then the code parameters, on its various derivatives, can be stored onboard and there is no need for re-distribution when the network changes. This, however, is not the general case that we consider in this work.

- 2) **Static Network Code.** *Static network coding* [4], [8] is an approach that enables a network code to account for different **pre-defined** topology configurations, denoted by $\varepsilon \in \hat{\varepsilon}$. For each configuration ε , a subset of edges $E_\varepsilon \subseteq E$ remain, and all the other edges are omitted from the network, so that the graph is $G_\varepsilon = \{V, E_\varepsilon\}^2$. A static code with respect to G and $\hat{\varepsilon}$, could operate under any configuration $\varepsilon \in \hat{\varepsilon}$, but it requires working over a field \hat{F} , which is growing proportionally to the number of configurations in $\hat{\varepsilon}$ (One field element has to be added for each pair of configuration-sink (ε, t) such that under ε , the paths from the source to t differ from those in the other configuration) [17]. If a network behaves in a predictable manner, then the network dynamics can be taken into account; it enables us to consider the network over τ time intervals as τ configurations derived

²if one would have wanted to be prepared for a node failure, the configuration would include the subset of edges that are not adjacent to this node.

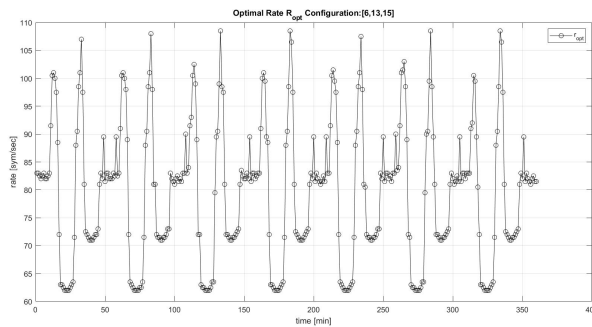
from a "unified" network, defined as $\bigcup_{t=1}^{\tau} G_{\varepsilon_t} = \{V, \bigcup_{t=1}^{\tau} E_{\varepsilon_t}\}$ (ε_t denoting the *links-failure* configuration during time interval $1 \leq t \leq \tau$). Using the unified network approach, and regarding all possible network topologies as links-failure configurations, enables one to deal not only with link-failures, but also with link additions. The main shortcoming of the static network coding approach, as will be later shown when the methods are compared, is the significantly larger field size it requires, which results with a corresponding reduction in communication rate.

- 3) **Intersection Network Code.** Another possible approach for coping with the network dynamics is to use only the links that exist for all the network configurations during a time interval τ . According to this approach, the network code is designed based on an effective network given by: $\bigcap_{t=1}^{\tau} G_{\varepsilon_t} = \{V, \bigcap_{t=1}^{\tau} E_{\varepsilon_t}\}$. Using this method, the field size does not change even though the network is dynamic - yet the communication rate is smaller as a result of the reduction in the max-flow. The trade off in choosing τ is clear: too large τ results with a relatively small communication rate due to low achievable max-flow (in case the network changes considerably over time); too small τ waists channel resources by needing to re-distribute updated code parameters.

A. Achievable Communication Rate - Upper Bound

Prior to comparing the aforementioned methods, first, an upper bound on the communication rate r_{opt} , given by the instantaneous network-code communication rate, is calculated for an example scenario and drawn in Figure 7.

Figure 7: Optimum rate upper bound from the source to sinks $\{6,13,15\}$. Simulation interval: $t = 0$ to $t = 360$ [min.]



The max-flow is calculated according to [2], where input link weights are set by eq. 2. The overall rate is calculated by dividing the max-flow value by $\lceil \log_2 |F| \rceil$, the bit rate induced by the field F . The observed max-flow periodicity over time is of course a consequence of the network-topology periodicity.

Note: the sinks are numbered in a sequential order, such that the nodes in the first plane are numbered 1 – 11, the second 12 – 23 etc. Adjacent nodes in a plane are numbered sequentially, hence node pairs $\{1, 12\}$, $\{2, 13\}$ etc. represent the same positions within the planes. The sinks used in the simulation shown in Figure 7 are taken from two different planes $\{2, 6\}$ & $\{13\}$.

B. Identifying the best Coding Scheme

Next, we proceed to compare the aforementioned coding approaches - using the methodology of *static network codes*, and *intersection network codes*, along with an introduction of *network interval-rate*.

1) Network Static and Intersection Rates:

Definition 9. *Network static rate* $r_{static}(\tau)$ with respect to the static configuration $\varepsilon = \{\epsilon_1, \epsilon_2, \dots, \epsilon_\tau\}$ is the network overall throughput³ assuming all path variations are considered as static links at network initialization (i.e, at $\tau = 0$), hence increasing the size of the field F . $r_{static}(\tau) =$

³since this is a *linear multicast* framework, the throughput of all designated sinks is the same, hence w.l.o.g. we have chosen to focus our discussion from a single-sink perspective.

$\frac{\sum_{\xi=1}^{\tau} h(\xi)}{\log(|F(\hat{\tau})|)}$ [symbols/sec] where $h(\xi)$ is the max-flow of the network for configuration ϵ_{ξ} , and $|F(\hat{\tau})| > |F| \cdot \tau$.

Definition 10. *Network intersection rate* $r_{intersection}(\tau_1, \tau_2)$ is the overall network throughput when using the intersection network $\bigcap_{t=\tau_1}^{\tau_2} G(t)$, inducing $r_{intersection}(\tau_1, \tau_2) = \frac{h_{int}(\tau_1, \tau_2)}{\log|F|}$, where $h_{int}(\tau_1, \tau_2)$ denotes the max-flow of $\bigcap_{t=\tau_1}^{\tau_2} G(t)$.

When examining $r_{intersection}(0, \tau)$ in the case of our example network, one can identify in Figure 10 that the rate stabilizes after a relatively short period of time. This implies that a significant portion of the network is practically fixed. Denote this “stable” max-flow value by h_{int}^{stable} corresponds to a “stable” rate $r_{intersection}^{stable}$.

Corollary 11. *In the example Iridium-based network, there exists a set of h_{int}^{stable} paths denoted by P , where $p_1, \dots, p_{h_{int}^{stable}} \in P$ are fixed under network dynamics. Note: this set is not necessarily expandable such that the addition of $p_{h_{int}^{stable}+1}, \dots, p_{h(\tau)}$ will achieve the network’s max-flow at time instance τ .*

The next example is aimed at demonstrating 11 and show that the addition of $p_{h_{int}^{stable}+1}, \dots, p_{h(\tau)}$ will not achieve the network’s max-flow at time instance τ .

Example 12. Let us examine the time-varying butterfly network depicted in Figure 8. At $t = 1$ (Figure 8a) links #4,5 are missing from the graph (but do appear at $t = 2$). Thus, the only path available to approach sink node #6 is $P_1^1 = \{1 \rightarrow 3 \rightarrow 7 \rightarrow 8\}$ (the numbering refer to the **edges**) while the paths to sink #7 achieving a max-flow (of 2) are $P_1^2 = \{2 \rightarrow 6\}$, $P_2^2 = \{1 \rightarrow 3 \rightarrow 7 \rightarrow 9\}$ achieving $h_6 = 1$, and $h_7 = 2$. It is easy to see that at $t = 2$, Figure 8b, the achievable max-flow is 2 for both sinks, i.e. $h_6 = h_7 = 2$ is possible. In order to achieve max-flow, edge #1 and edge #7 must be in **different** paths (otherwise employment of path $\{1 \rightarrow 5\}$ is impossible, essential for achieving max-flow). Thus, changing P_1^1 is a necessity.

Figure 8: Time-varying butterfly network

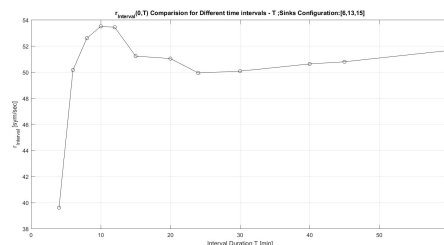


2) Network Interval Rate:

Definition 13. *Network interval rate* $r_{interval}(\tau, T)$ is the (average) network throughput in interval time τ assuming the network code parameters must be re-distributed over the entire network once every sub-interval time T , $\tau < T$. The base rate within the k 'th sub-interval is the network intersection rate $r_{intersection}(\tau_1, \tau_2)$ for $\tau_1 = (k - 1) \cdot T$, $\tau_2 = kT$. The overall rate is defined as the average on the entire interval T (including the distribution time): $r_{interval}(\tau, T) = \frac{\sum_{k=1}^{\tau/T} r_{intersection}((k-1) \cdot T, kT) \cdot (1 - \frac{t_{distribution}}{T})}{\tau/T} = \sum_{k=1}^{\tau/T} r_{intersection}((k-1) \cdot T, kT) \cdot (\frac{T - t_{distribution}}{T})$

where $t_{distribution}$ is the time required for re-distributing the tailored code-parameters throughout the entire network (see Equation 3).

Figure 9: Interval-Rate performance as a function of the sub-interval time T ; single source, sink nodes are $\{6, 13, 15\}$. Optimum rate is achieved for $T = 10[min]$.



As demonstrated in Figure 9, there exists a certain *sub-interval time* T , achieving the optimum Network interval rate. In fact, in many of the examined configurations such optimum exists. In

addition, we note that for very long sub-intervals, the network interval rate almost coincides with the network intersection rate.

Definition 14. Let t_{period} be the period time of r_{opt} , meaning $t_{period} = t_{peak_{\#n+1}} - t_{peak_{\#n}}$. For example, Figure 7 shows a peak in $t_{peak_{\#1}} = 30m$, and $t_{peak_{\#2}} = 80m$ resulting $t_{period} = 50m$.

Definition 15. Let τ_{stable} denote the time achieving a stable *intersection rate* $r_{intersection}(t_0, \tau)$, with t_0 being the simulation's start time.

$$\tau_{stable} = \min\{\tau | r_{intersection}(\tau, \infty) > \text{precentile90}(r_{intersection}(0, \infty))\}.$$

It is important to set this criterion and not arbitrarily choose t_{period} since in some of the cases there is a strong dependency on the initialization conditions (the choice of t_0) such that the upper bound for relaxation is $2 \cdot \tau_{period}$.

Definition 16. Let T_{opt} denote the (*optimal*) *sub-interval time* T that results with the best achievable *stable rate* $r_{interval}(\tau, T)$ for different T 's. $T_{opt} = \underset{\tau_{stable} \leq T \leq \tau}{max} \{r_{interval}(\tau, T) | \tau > \tau_{stable}\}$ i.e, comparing different T 's after τ_{stable} . 9 shows the comparission of different T 's (rates are after τ_{stable}), we can clearly see that $T_{opt} = 10m$ in the example herein.

3) *Techniques Comparison:* In order to identify which is the best network coding technique, we shall compare the following rates: $r_{intersection}$, $r_{interval}(T_{opt})$, and r_{opt} (r_{opt} being the upper bound demonstrated in Figure 7).

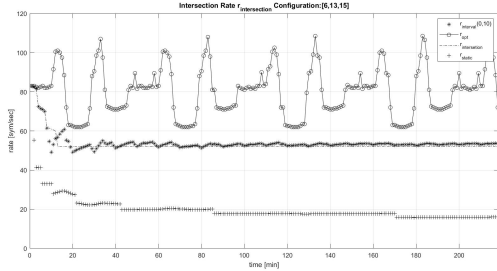
It is interesting to note that for the majority of the studied topologies and sink configurations, optimal value T_{opt} exists, namely $r_{interval}(\tau, T_{opt})$ outperforms all the other network coding techniques. For all the other studied topologies, no specific T_{opt} value was found, and $r_{interval}$ monotonically increases with the sub-interval length T such that $r_{interval}(\tau, T_{opt}) \rightarrow r_{intersection}(\tau, \infty)$.

C. On the Existence of T_{opt}

Since the *interval rate* was identified as the best network coding scheme if specific T_{opt} exists, it certainly is desirable to determine whether such T_{opt} exists without having to explicitly design

Figure 10: Techniques comparison: left figure - the interval rate with $T = 10[min]$ outperforms the intersection rate; right figure - the intersection rate outperforms the interval rate for any selection of *sub-interval time* T .

(a) sinks: $T = \{6, 13, 15\}$ the interval rate with $T = 10[min]$



(b) sinks: $T = \{15, 17, 19\}$ - the intersection rate outperforms the interval rate for any selection of *sub-interval time* T .

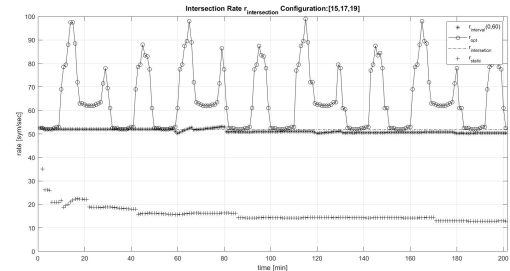
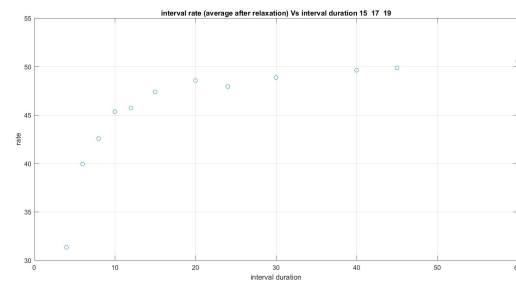
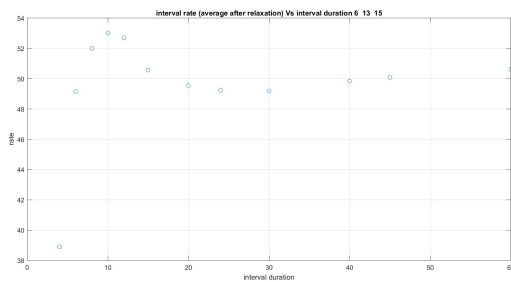


Figure 11: $r_{interval}$ for different sink sets T in both configurations

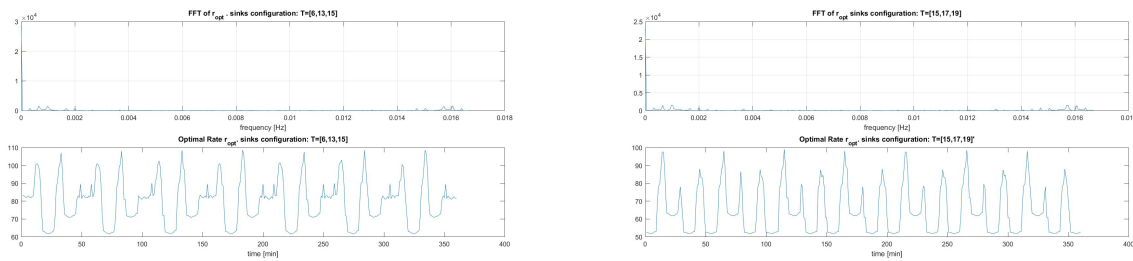


the network code. In this section we outline criteria for addressing this problem.

Example 17. Let us compare two network configurations: one with the set of sinks $T = \{6, 13, 15\}$ and the other with sinks $T = \{15, 17, 19\}$ demonstrated in Figure 11.

We clearly note that the configuration with $T = \{6, 13, 15\}$ has a distinct optimum $r_{interval}$ for $T_{opt} = 10[min]$, while the rate in the configuration $T = \{15, 17, 19\}$ is monotonously increasing such that $r_{interval} \rightarrow r_{intersection_{inf}}$. This short example is very interesting because two quite similar topologies (3 sinks, same source) need different coding scheme. One difference between the configurations is that sinks $\{15, 17, 19\}$ are all in the same orbital-plane, while $\{6\}$ and $\{13, 15\}$ are not. However, other cross-plane sink configurations didn't necessarily result in the same outcome, meaning there is a more profound difference we must indicate. We tried to build

Figure 12: Examining Time and Frequency Domain Characteristics of Both Topologies



a model that is based on time and frequency domain properties of the network instantaneous max-flow (i.e. r_{opt}) which is a direct result of the network topology to find this criterion.

Example 18. Let us examine r_{opt} of the two configurations as presented in 12.

$r_{interval}(\tau, T)$ as defined in 13 does not take only the maximum value of r_{opt} , but is also influenced by the r_{opt} peak width, and number of peaks. Thus, examining the signal also in the frequency domain (observing the Fourier transform of r_{opt}) is desired. Unfortunately there was no correlation between configurations that yields T_{opt} and those that don't.

This forces us to look for different criteria, in the time domain, but rather than employing only the maximum max-flow values, we shall also consider different percentiles of r_{opt} suggesting how long does a certain topology is above a specific value:

- 1) $PAPR$ denotes the peak-to-average ratio of $r_{opt}(\tau)$; $PAPR = \frac{\max(r_{opt}(\tau))}{\text{mean}(r_{opt}(\tau))}$.
- 2) $maxRa$ denotes the maximum of $r_{opt}(\tau)$ during the simulation; $maxRa = \frac{\max\{r_{opt}(\tau)\}}{r_{intersection}}$
- 3) $rateR$ denotes the maximum of $r_{interval}(\tau, T_{opt})$ during the simulation; $rateR = \frac{\max(r_{interval}(\tau, T))}{r_{intersection}}$
- 4) $p50$ denotes the ratio $p50 = \frac{\max(r_{opt}(\tau))}{\text{median}(r_{opt}(\tau))}$.
- 5) $p75$ denotes the ratio Median $p75 = \frac{\max(r_{opt}(\tau))}{\text{percentile75}(r_{opt}(\tau))}$

other variations of percentiles were examined (80%, 90%, 25%), they didn't result different outcomes, thus weren't mentioned specifically.

$rateR$ represents our "unit under test", $rateR < 1$ values represents configuration without T_{opt} . In order to compare the different techniques, other criteria were also set to be unit-less. $PAPR$ represents the "classical" criterion comparing peak to average, while $p50$, and $p75$ increase the

importance of the rate distribution (i.e. testing for how long the signal stays at higher rates). $maxRa$ emphasizes only the peak value of the specific configuration.

Figure 13: Correlation Matrix between Different Topology Criteria

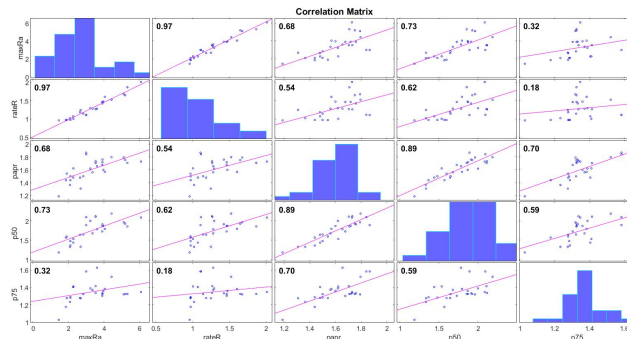


Figure 13 shows a comparison between the correlations of the different criteria presented for 29 different configurations (varying number of sinks, number of orbital-planes). As can be seen in Figure 13, the strongest correlation between $rateR$ to any other criterion is to $maxRa$, hence implying a connection, and a desire to test for a specific threshold determining rather T_{opt} exists. This result supports the lack of correlation in the frequency domain analysis since inhere too, the criterion chosen ($maxRa$) does not express any temporal aspect unlike $p50$ or $p75$. This is quite surprising since $r_{interval}(\tau, T)$ by definition has a strong time dependency.

Setting the Threshold: In Figure 13 we focus on the histogram of the chosen criterion $maxRa = \frac{max\{r_{opt}(\tau)\}}{r_{intersection}}$ compared to $rateR = \frac{max(r_{interval}(\tau, T))}{r_{intersection}}$. We can clearly see, that configurations with the ratio $maxRa < 2$ are more likely to not have an optimum for $r_{interval}(0, T)$ (the corresponding configurations have $rateR < 1$).

Figure 14: Correlation Examination to Set Threshold for Different Configurations. black line: maxRa, blue line: rateR

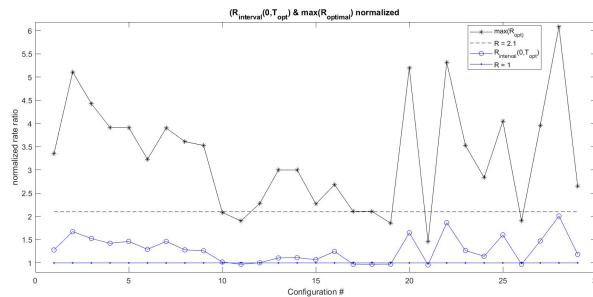


Figure 14 shows that the correlation presented in Figure 13 indeed indicates that a configuration with no distinct $r_{intersection}(0, T)$ maxima (i.e. with no T_{opt} , resulting with $rateR < 1$) has a $\frac{max(R_{opt})}{R_{intersection}(0, \infty)} < 2.1$ ratio.

To conclude this section, not only that better approaches than *static network coding* were presented for dealing with topology variations, but an efficient way of finding the most appropriate coding scheme was advocated. Determining whether a certain configuration has an optimal T_{opt} is the key, and it no longer requires computing all different options of $r_{interval}(\tau, T)$, but only computing $max(r_{opt})$, and $r_{intersection}(0, \infty)$. This suggested test is based on 29 different sink configurations intended for spanning all sorts of topological aspects of the network (sink numbers, cross orbital-planes combinations). Nevertheless, the threshold for the suggested test might change under new configurations, this without decreasing the strength of this criterion.

VI. CONCLUSION

A schematic implementation of network coding was presented for a swarm of communicating satellites, conceptually based on the Iridium system. Close-to-realistic network dynamics model and its parameters have been derived from the Systems Tool Kit (STK) simulation environment. In particular, we introduced the notion of *generalized acyclic network*, which promoted effective generation of *linear network codes* for what was considered until now to be a cyclic network.

One of the major challenges of network coding under realistic network conditions is the dynamic changes that the network experiences over time. To cope with this challenge, several

methods were suggested and compared, among these is the known *static network coding* approach that is traditionally used to tackle link failures. It was demonstrated that in all cases, relating to our chosen example network, static network codes under-performed compared to the methods presented. Importantly, a simple test was formulated so as to be able to determine which of the coding schemes is best to employ in a given scenario. The test is based solely on the topology of the network, more explicitly - the relation between the peak max flow of the network and the max flow of the *intersection network*.

REFERENCES

- [1] R Alshwede, N Cai, S.-Y Li, and R Yeung. Network information flow: Single source. *IEEE Trans. Inform. Theory*, 2000.
- [2] Yuri Boykov and Vladimir Kolmogorov. An experimental comparison of min-cut/max-flow algorithms for energy minimization in vision. *IEEE transactions*, 26:1124–1137, 2004.
- [3] Elona Erez and Meir Feder. Efficient network code design for cyclic networks. *IEEE Transactions on Information Theory*, 56:3862–3878, 2010.
- [4] S Fong and R Yeung. Variable-rate linear network coding. pages 409–412, 2006. Oct. 2006.
- [5] L. R. Ford and D. R. Fulkerson. Flows in networks. *UNITED STATES AIR FORCE PROJECT RAND*, 1962.
- [6] El Gamal, Abbas, and Young-Han Kim. Cambridge university press, 2011.
- [7] Sidharth Jaggi. Polynomial time algorithms for multicast network code construction. *IEEE Transactions on Information Theory*, 51:1973–1982, 2005.
- [8] R Koetter and M Medard. An algebraic approach to network coding. *IEEE/ACM Trans. Netw*, Oct. 2003.
- [9] S Li, R Yeung, and N Cai. Linear network coding. *IEEE Trans. Inform. Theory*, 49:371, Feb. 2003.
- [10] Shuo-Yen Li, Raymond Robert, and null Yeung. On convolutional network coding. 2006. 2006.
- [11] Muri and J Mcnair. A survey of communication sub-systems for intersatellite linked systems and cubesat missions. *J. Commun*, 7(4):290–308, Apr. 2012.
- [12] O Popescu, J Harris, and D Popescu. Designing the communication sub-system for nanosatellite cubesat missions: Operational and implementation perspectives. pages 1–5, 2016. March. 2016.
- [13] Otilia Popescu. A technical comparison of three low earth orbit satellite constellation systems to provide global broadband. October 2018.
- [14] Stephen Pratt. An operational and performance overview of the iridium low earth orbit satellite system. *IEEE Communications Surveys*, 2:2–10, 1999.
- [15] R Radhakrishnan. Survey of inter-satellite communication for small satellite systems: Physical layer to network layer view. *IEEE Commun. Surveys Tuts*, 18(4):2442–2473, 2016.
- [16] Christian Rodriguez, Henric Boiardt, and Sasan Bolooki. Cubesat to commercial intersatellite communications: Past, present and future. In *IEEE Aerospace Conference*. IEEE, 2016. 2016.

- [17] QIFU TYLER SUN. On construction of variable-rate and static linear network codes. *IEEE Access*, 2018.
- [18] R Yeung, S.-Y. Li, and N Cai. *Network Coding Theory (Foundations and Trends in Communications and Information Theory)*. Now Publishers, Hanover, MA, 2006.